ACS Energy LETTERS

http://pubs.acs.org/journal/aelccp

LETTER

Quantum Mechanics Reactive Dynamics Study of Solid Li-Electrode/Li_6PS_5Cl-Electrolyte Interface

Tao Cheng,[†] Boris V. Merinov,[*,†] Sergey Morozov,[‡] and William A. Goddard, III[†]

[†]Materials and Process Simulation Center, MC 139-74, California Institute of Technology, Pasadena, California 91125, United States

[‡]South Ural State University, 76 Lenin Avenue, Chelyabinsk 454080, Russia

Supporting Information

ABSTRACT: We have performed a theoretical study of the Li/Li_6PS_5Cl interface and showed the ability of the applied computational methods to properly describe the chemical processes that occur at the interface. After a 500 ps ab initio molecular dynamics simulation, we find that the Li/Li_6PS_5Cl interface decomposes with formation of multiple phases and that the main decomposition products are Li_2S, Li_3P, LiCl, and possibly LiP. These findings are in good agreement with reported experimental data. The observed quick decomposition is attributed to the weak bonding between P and S. On the basis of this and earlier obtained experimental results, we conclude that the chemical instability may be an intrinsic problem of P−S-based solid electrolytes when they are in contact with Li-metal. Our results validate the effectiveness of the available computational tools to reach a deeper insight into the evolution of interfacial structures and properties prior to experiment.

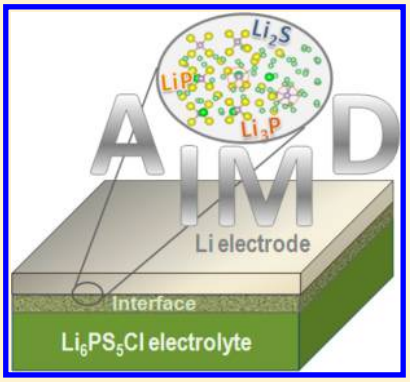

Solid-state electrolytes are being explored intensively as the key component in developing all-solid-state batteries.[1−5] They could provide a number of advantages over the currently used liquid Li-ion battery technology, including faster charging, higher energy density, increased cycle life, reduced battery costs, and greater flexibility with regard to battery placement and vehicle design. Several sulfide glasses, glass-ceramics, and ceramics have been developed as promising electrolytes, mainly based on binary and ternary systems, including Li_2S−P_2S_5[6,7] with ternary components such as P_2S_3, GeS_2, and P_2O_5. Currently, $Li_{10}GeP_2S_{12}$ exhibits one of the highest lithium ionic conductivities, 1.2×10^{-2} S/cm at room temperature,[8,9] among Li-conducting solid electrolytes. However, $Li_{10}GeP_2S_{12}$ contains germanium, whose abundance in the earth's crust is very low, making it too expensive. In addition, $Li_{10}GeP_2S_{12}$ was shown to be unstable in contact with Li-metal electrode, decomposing to form Li_3P, Li_2S, and Li−Ge alloys at the Li/$Li_{10}GeP_2S_{12}$ interface.[10]

Another promising sulfide-based glass-ceramic in the Li_2S−P_2S_5 system is $Li_7P_3S_{11}$, which has a very high ionic conductivity of $\sim 10^{-2}$ S/cm at room temperature as well.[6,11,12] Unfortunately, as shown in ref 12, this material is also unstable in contact with Li metal, decomposing to products such as Li_2S and Li_3P and possibly LiP, LiP_5, and LiP_7. This causes degradation of the interfacial properties, resulting in deterioration of battery performance.

Other prospective sulfide ceramic materials, which can be considered as providing a balance between efficiency and price, belong to the Li-argyrodite Li_6PS_5X (X = Cl, Br, I) family. They also exhibit superionic conductivity of $\sim 10^{-2}$ S/cm at room temperature.[13−15] An all-solid-state Li-ion battery $LiCoO_2$/Li_6PS_5Cl/Li_4Ti_5O was assembled and demonstrated to be capable of operating at room temperature.[16] However, upon cycling, growth of a resistive layer at the $LiCoO_2$/Li_6PS_5Cl interface was detected, limiting the battery performance.

These results make it clear that the electrode/electrolyte interface remains the most critical part of electrochemical devices. The reported data[10,12,16] indicate the importance of studying the stability of the electrode/electrolyte interface before solid electrolyte materials would be recommended for application in Li-batteries. To learn more about the interfacial chemistry, we selected Li_6PS_5Cl as a representative of the Li-argyrodite family and examined the Li/Li_6PS_5Cl interface structure and stability using quantum mechanics (QM) and ab initio molecular dynamics (AIMD) simulations.

The cubic crystal structure of Li_6PS_5Cl is shown in Figure 1a. The 48*h* crystallographic position of space group $F\bar{4}3m$ with occupancy coefficient 0.5 plays a key role in the diffusion paths of the mobile Li-cations. To create a cell with the disordered Li-sublattice, we first randomly removed half of the Li atoms. The obtained structure is shown in Figure 1b. DFT calculations

Received: April 13, 2017
Accepted: May 23, 2017
Published: May 23, 2017

DOI: 10.1021/acsenergylett.7b00319
ACS Energy Lett. 2017, 2, 1454−1459

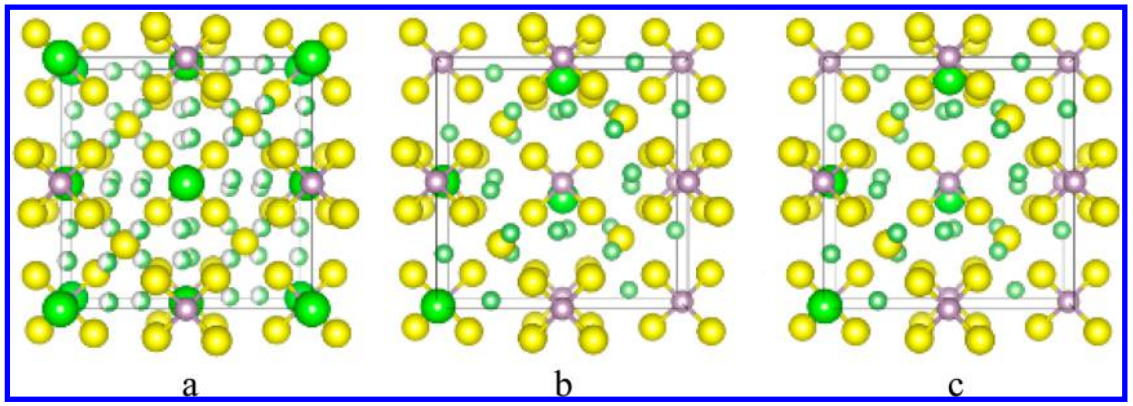

Figure 1. (a) Experimental cubic (space group $F\bar{4}3m$) crystal structure of Li_6PS_5Cl. The Li sites are partially occupied (50%), which create vacancies to facilitate the fast Li-ion diffusion. The formal charges are +1, + 5, −2, and −1 for Li, P, S, and Cl, respectively. (b) The structure after randomly removing half of the Li atoms, and (c) the crystal structure after QM optimization. Li, light green balls; P, purple balls; S, yellow balls; and Cl, darker green balls.

were carried out at the level of PBE to optimize the crystal structure. For details on our DFT computation, see the Supporting Information. The QM optimized structure is shown in Figure 1c, which is very similar to the experimental structure, with cell parameters close to the experimental values (Table 1). This validates that our constructed structure provides a reasonable starting point for further calculations.

Table 1. Comparison of the Simulated Cell Parameters (Å), Angles (degree), and Volume (Å^3) (DFT PBE) to Experimental Values

method	*a*	*b*	*c*	*α*	*β*	*γ*	volume
QM	10.16	10.11	10.16	91.6	89.8	91.6	1042.38
exptl	10.15	10.15	10.15	90	90	90	1045.68

Next, we built a Li/Li_6PS_5Cl system to investigate the interface between solid electrolyte and electrode (Figure 2a). The model system consists of eight layers of Li [BCC structure with a 3 × 3 (100) surface] and six layers of Li_6PS_5Cl with the (100) surface, totaling 228 atoms. The optimized cell length of the Li BCC structure is 3.44 Å. Therefore, the corresponding 3 × 3 (100) surface has a supercell length of 10.32 Å with a surface area of 106.50 Å^2. The Li (100) surface closely matches the 10.15 Å cell length and 103.02 Å^2 surface area of the Li_6PS_5Cl (100) surface. This system was used in our further computations.

During QM (DFT PBE) optimization (energy minimization), PS_4 at the interface quickly decomposed, breaking P−S bonds and forming new P−Li and Li−S bonds. Figure 2b shows the atomic structure after optimization. The calculated radial distribution function (RDF) confirms the above-mentioned bonding changes (Figure 3). The intensities of the P−S peaks decrease, while new P−Li peaks appear in a shorter distance range (2−3 Å). Integrating the RDF shows that the number of S atoms coordinated to P decreases, and simultaneously the number of Li atoms coordinated to P increases. The S atoms penetrate into the Li negative electrode forming a new Li−S interaction at the cost of breaking of the Li−S bonds in the Li_6PS_5Cl solid electrolyte. This in turn affects the Li−S RDF. Similar changes are observed in the Li−Cl RDF, where the peak intensities significantly decrease with simultaneous broadening, and the Li atom coordination becomes slightly higher, most probably because of the breaking of the Li−Cl bonds in Li_6PS_5Cl and formation of new ones.

Because the decomposition occurs during the optimization, we conclude that the corresponding reactions have very low or no energy barriers, indicating that Li_6PS_5Cl is unstable in contact with Li metal. The observed quick decomposition can be attributed to the weak bonding between P and S. On the basis of our computations and earlier experimental results,[10,12] we conclude that the chemical instability is probably an intrinsic problem of P−S-based solid electrolytes in contact with Li-metal.

A possible solution might be partial oxidation of the interface, using more stable P−O bonds to replace the weak P−S bonds. Of course, introducing the P−O bonds will inevitably decrease the ionic conductivity of the system. Therefore, the oxidized layer should be sufficiently thin so that the overall conductivity of the system would not be reduced to an unacceptable value. Figure 2c shows the initial Li/Li_6PS_5Cl system with the partially oxidized interface. After the QM energy minimization, no decomposition was observed.

To further investigate the stability of the Li/Li_6PS_5Cl system with the partially oxidized interface, we carried out AIMD at 298 K, with the volume fixed (*NVT*). More details on our AIMD computations are given in the Supporting Information. We found that the system remains stable for 100 ps of simulation, but it began to decompose at longer times. Thus, the partial oxidation improves the endurance of the Li/Li_6PS_5Cl interface, but it does not eliminate the interface instability problem.

To reach a deeper insight into the Li/Li_6PS_5Cl interface degradation process, we carried out a series of 500 ps AIMD simulations at three different temperatures: 298, 398, and 498 K. The use of higher temperature accelerates the possible reactions to a time scale practical for AIMD. The corresponding interface structures are shown in Figure 4. Even in the simulation at 298 K, we observe significant interface decomposition after 500 ps. The primary reaction can be described as the following:

$$(x + 5y + z - 6)\mathrm{Li} + \mathrm{Li_6PS_5Cl} \rightarrow \mathrm{Li}_x\mathrm{P} + 5\mathrm{Li}_y\mathrm{S} + \mathrm{Li}_z\mathrm{Cl}$$

Here metallic Li from the electrode is oxidized to Li^+ to supply one electron, while P^{5+} is reduced to P^{3+} by breaking the P−S bond. Then the newly formed Li^+ diffuses into the electrolyte, while P^{3+}, S^{2-}, and Cl^- diffuse to a lesser extent

DOI: 10.1021/acsenergylett.7b00319
ACS Energy Lett. 2017, 2, 1454−1459

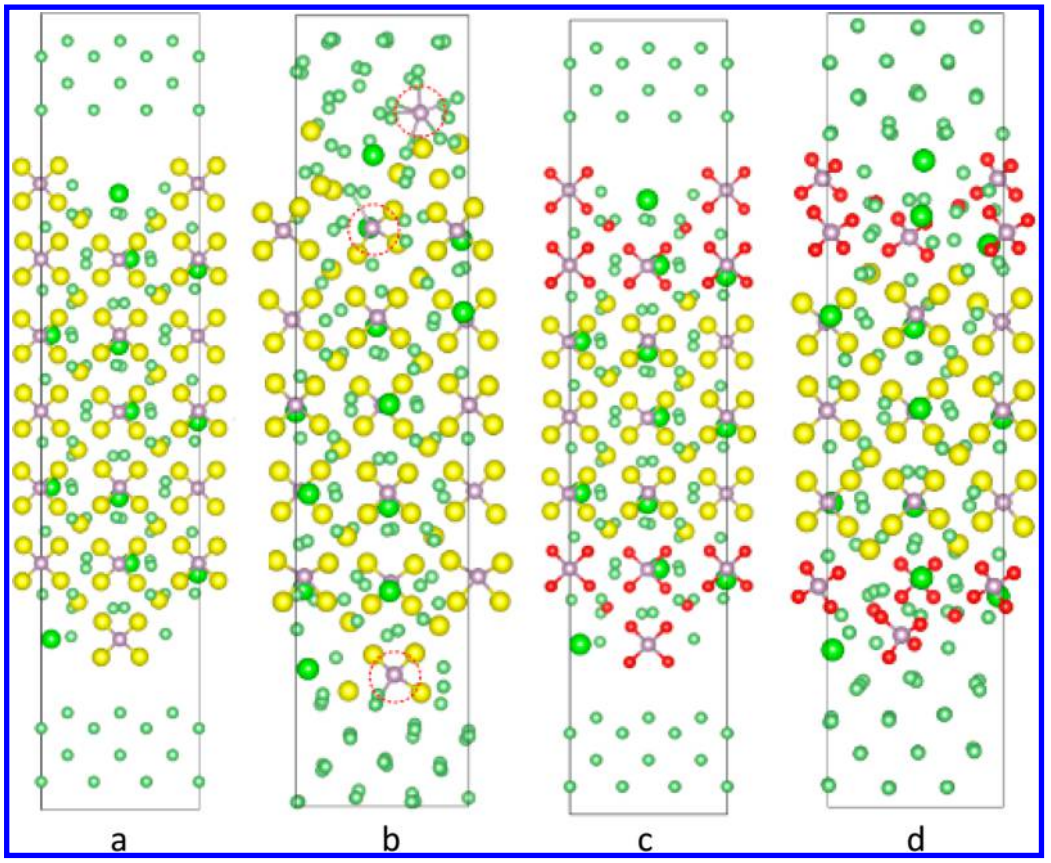

Figure 2. Atomic structure of the (a) initial solid Li-electrode/Li_6PS_5Cl-electrolyte system and (b) after QM (DFT PBE) optimization; (c) initial Li/Li_6PS_5Cl system with the partially oxidized interface and (d) after QM (DFT PBE) optimization. Oxygen atoms are shown by red balls. The red dashed circles highlight decomposed PS_4 tetrahedra. The other notations are the same as in Figure 1.

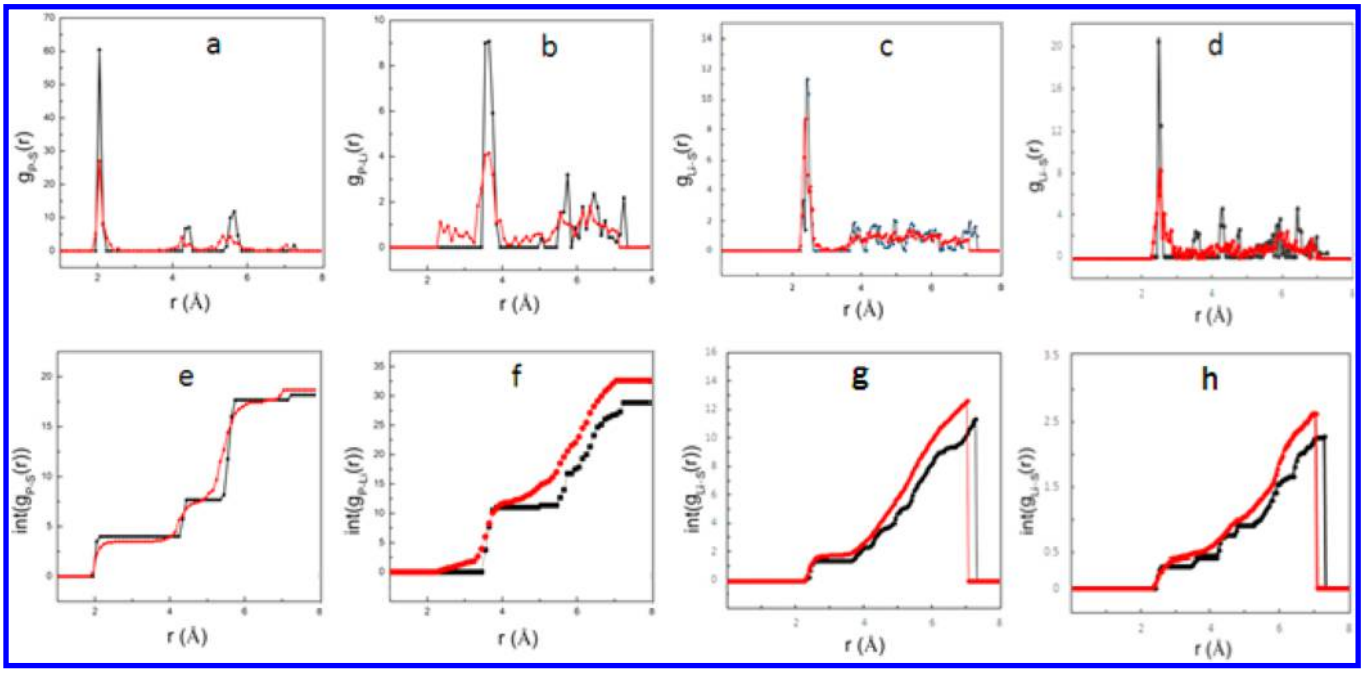

Figure 3. Radial distribution functions (RDF), $g(r)$, of (a) P−S, (b) P−Li, (c) Li−S, (d) Li−Cl distances. Panels e, f, g, and h are their integrations, respectively, for the "as-built" interface (black line) and interface after QM optimization (red line).

along the opposite direction into the electrode. These reactions have very low energy barriers (or no energy barriers at all), because they are observed directly even in the simulation at room temperature. Most probably, these reactions are diffusion-controlled. Therefore, given enough time, the entire electrolyte will be reduced to Li_xP and Li_yS phases, if sufficient Li is available. These assumptions are supported by our higher-temperature AIMD simulations. We find that more pronounced

DOI: 10.1021/acsenergylett.7b00319
ACS Energy Lett. 2017, 2, 1454−1459

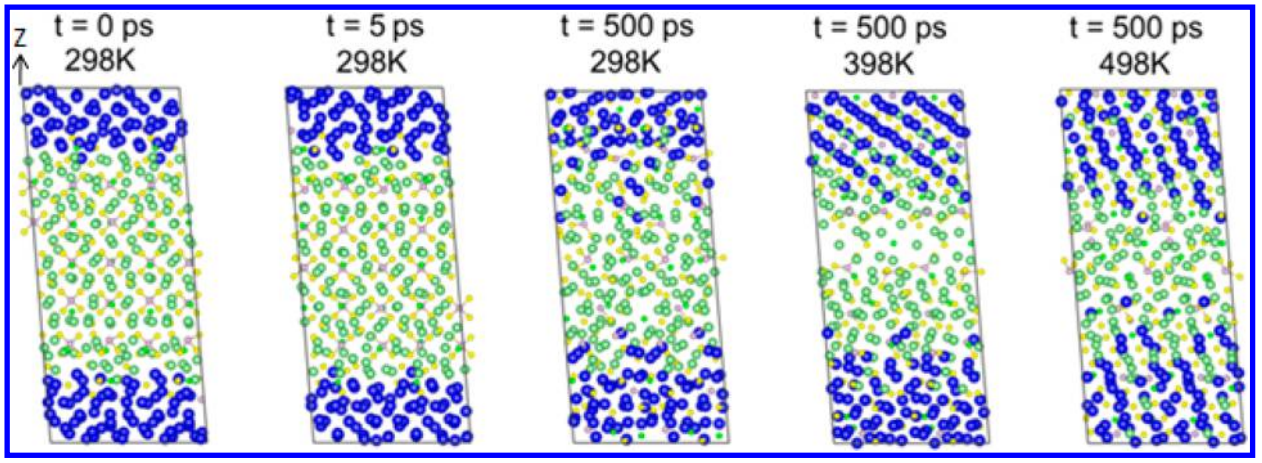

Figure 4. Degradation of the Li-electrode/Li_6PS_5Cl-electrolyte interface from *NVT* AIMD. Li-metal (electrode), blue balls. The other notations are the same as in Figure 1.

surface decompositions take place at 398 and 498 K. Interestingly, the surface reconstruction occurs together with the surface reactions leading to clear crystallized boundaries being formed approximately along the z direction (see Figure 4).

Figure 5 shows the density distributions of the P, S, and Cl atoms along the z direction at T = 498 K. It is clearly seen that

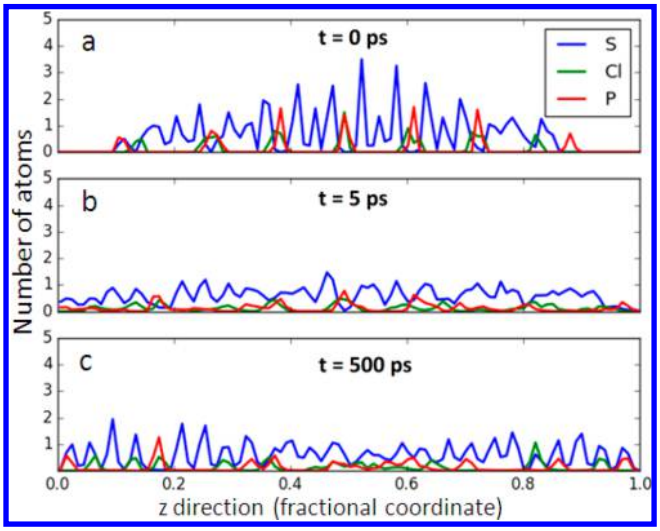

Figure 5. Density profiles of S, Cl, and P at different simulation times from the AIMD simulation at T = 498 K.

the P and Cl peaks are overlapped in the bulk at t = 0 ps, whereas the peaks correspond to P and Cl close to the Li-electrode surface (interface) are separate (Figure 5a). It means that the P and Cl atoms occupy positions with similar z coordinates in bulk and different in the interface. The latter is because of the initial electrode−electrolyte chemical reactions during the system optimization process. After 5 ps of AIMD (Figure 5b), the crystallinity of the system is significantly reduced because of further proceeding of the electrode−electrolyte reactions, and some minor atomic diffusion into the Li-electrode is observed. However, after 500 ps of simulation (Figure 5c), the system again demonstrates a better crystallinity, in particular in the electrode and interface regions (between 0.0 and 0.35 and between 0.75 and 1.0). The peaks also indicate appreciable atomic diffusion into the electrode.

The previously observed overlapping of the P and Cl peaks at t = 0 ps (Figure 5a) almost disappears. This is most probably a consequence of the formation of new phases which are mixed with each other. The simulated XRD patterns (Figure 6)

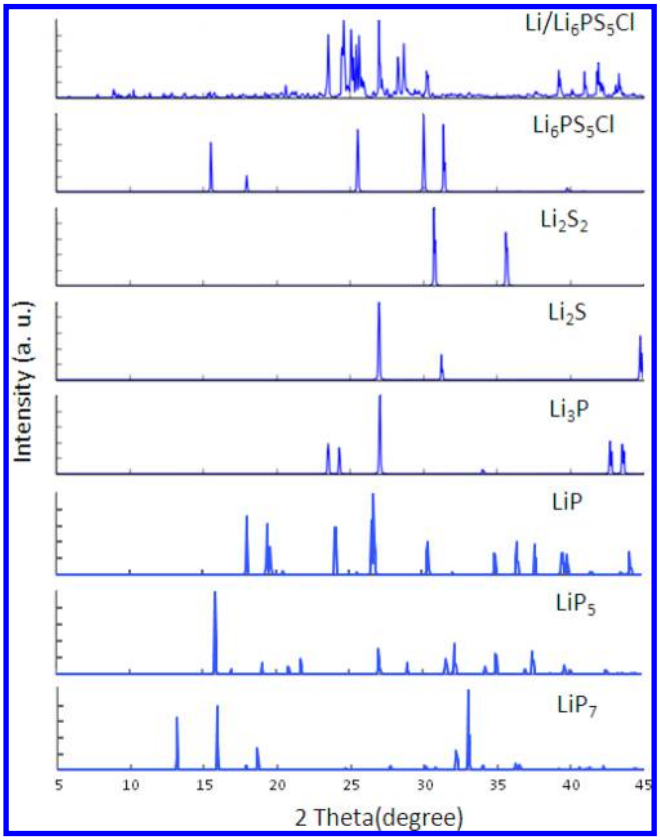

Figure 6. Simulated XRD patterns of the Li/Li_6PS_5Cl interface after a 500 ps AIMD at T = 498 K and possible decomposition products.

confirm that the interface consists of multiple phases, and the main decomposition products are Li_2S, Li_3P, and possibly LiP. These are in good agreement with reported experimental results on decomposition products found for the Li/$Li_{10}GeP_2S_{12}$ and Li/$Li_7P_3S_{11}$ interfaces.[10,12]

To complete the discussion, we will consider the role of Cl in the interface formation. It is generally accepted that the Li

DOI: 10.1021/acsenergylett.7b00319
ACS Energy Lett. 2017, 2, 1454−1459

metal negative electrode in Li-ion batteries is covered by a solid electrolyte interphase (SEI) containing LiCl,[17] if lithium perchlorate ($LiClO_4$) is used to prepare the electrolyte solution. We assume that LiCl is formed as a decomposition product in our Li/Li_6PS_5Cl system too. The corresponding XRD pattern (Figure 6) has the peak at $2\Theta = 30°$, which is characteristic for LiCl. However, the XRD pattern of Li_6PS_5Cl has the peak at a similar angle as well. To prove the LiCl formation, we calculated the Li−Cl RDFs from our AIMD simulation at $t = 0$ and 500 ps (Figure 7). The Li−Cl peaks for the first

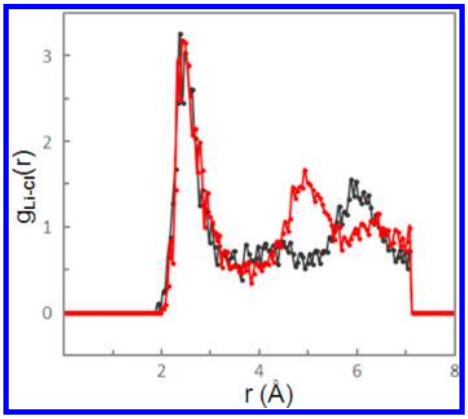

Figure 7. Radial distribution functions (RDF), $g(r)$, of the Li−Cl distances from the 498 K AIMD simulation at $t = 0$ ps (black line) and $t = 500$ ps (red line).

coordination sphere (at ∼2.5 Å) are practically overlapped for the system at $t = 0$ ps and $t = 500$ ps, which means that the number of the Li−Cl bonds remains the same. Thus, this peak is not informative enough for the goal of our analysis. Fortunately, the peaks for the second coordination sphere are suitable for the LiCl identification. Because of the different structural arrangements, a Li−Cl RDF peak for the second coordination sphere (at ∼4.5 Å at room temperature) should be much more intense for LiCl than that for Li_6PS_5Cl. The Li−Cl RDF of the system at $t = 0$ shows the peak at ∼6 Å, and there is no peak at ∼4.5 Å. After 500 ps of the AIMD simulation, the intensity of the 6 Å peak significantly decreased whereas the new peak appeared at ∼5 Å (the peak is shifted from 4.5 Å to a longer distance because of the higher temperature of the simulation, $T = 498$ K). We consider these changes in the Li−Cl RDF as evidence for the LiCl phase formation.

In summary, we used QM-based reactive molecular dynamics (RMD) to predict chemical reactions at the Li/Li_6PS_5Cl interface at different temperatures. We find that that the Li/Li_6PS_5Cl interface is unstable and decomposes quickly, forming multiple phases. Our attempt to stabilize the system by partial oxidation of the Li/Li_6PS_5Cl interface failed. The identified decomposition products are Li_3P, Li_2S, LiCl, and possibly LiP. These compounds have ionic conductivity that is much lower[18−20] than that of Li_6PS_5Cl.[13−15] The formation of such low ionic conductive products leads to deterioration in the transport properties of the whole system, resulting in degradation of battery performance. This implies the need for new electrolytes that are not sensitive to reactions with Li, perhaps such as highly ionic conductive polymeric, polymer−, and ceramic−ionic liquid materials.[21−26] Our study indicates that QM RMD has the potential to test new suggestions prior to synthesis and experimental characterization.

■ ASSOCIATED CONTENT

Supporting Information

The Supporting Information is available free of charge on the ACS Publications website at DOI: 10.1021/acsenergylett.7b00319.

A description of the computational methods applied (PDF)

■ AUTHOR INFORMATION

Corresponding Author

*E-mail: merinov@caltech.edu.

ORCID

Tao Cheng: 0000-0003-4830-177X
Boris V. Merinov: 0000-0002-2783-4262
Sergey Morozov: 0000-0001-6226-5811
William A. Goddard III: 0000-0003-0097-5716

Notes

The authors declare no competing financial interest.

■ ACKNOWLEDGMENTS

This work was supported by Bosch Energy Research Network Grant No. 13.01.CC11. We thank our Bosch colleague Dr. Boris Kozinsky for fruitful discussions and critical feedback on this work.

■ REFERENCES

(1) Braga, M. H.; Grundish, N. S.; Murchison, A. J.; Goodenough, J. B. Alternative Strategy for a Safe Rechargeable Battery. *Energy Environ. Sci.* **2017**, *10*, 331−336.
(2) Yue, L.; Ma, J.; Zhang, J.; Zhao, J.; Dong, S.; Liu, Z.; Cui, G.; Chen, L. All Solid-State Polymer Electrolytes for High-Performance Lithium Ion Batteries. *Energy Storage Materials* **2016**, *5*, 139−164.
(3) Santhanagopalan, D.; Qian, D.; McGilvray, T.; Wang, Z.; Wang, F.; Camino, F.; Graetz, J.; Dudney, N.; Meng, Y. S. Interface Limited Lithium Transport in Solid-State Batteries. *J. Phys. Chem. Lett.* **2014**, *5*, 298−303.
(4) Robinson, A. L.; Janek, J. Solid-State Batteries Enter EV Fray. *MRS Bull.* **2014**, *39*, 1046−1047.
(5) Munshi, M. Z. A. *Handbook of Solid State Batteries and Capacitors*; World Scientific Publishing Co., Pte, Ltd.: Singapore, 1995.
(6) Seino, Y.; Ota, T.; Takada, K.; Hayashi, A.; Tatsumisago, M. A Sulphide Lithium Super Ion Conductor is Superior to Liquid Ion Conductors for Use in Rechargeable Batteries. *Energy Environ. Sci.* **2014**, *7*, 627−631.
(7) McGrogan, F. P.; Swamy, T.; Bishop, S. R.; Eggleton, E.; Porz, L.; Chen, X.; Chiang, Y.-M.; van Vliet, K. J. Compliant Yet Brittle Mechanical Behavior of Li_2S−P_2S_5 Lithium-Ion-Conducting Solid Electrolyte. *Adv. Energy Mater.* **2017**, 1602011.
(8) Kamaya, N.; Homma, K.; Yamakawa, Y.; Hirayama, M.; Kanno, R.; Yonemura, M.; Kamiyama, T.; Kato, Y.; Hama, S.; Kawamoto, K.; et al. A Llithium Superionic Conductor. *Nat. Mater.* **2011**, *10*, 682−686.
(9) Hassoun, J.; Verrelli, R.; Reale, P.; Panero, S.; Mariotto, G.; Greenbaum, S.; Scrosati, B. A Structural, Spectroscopic and Electrochemical Study of a Lithium Ion Conducting $Li_{10}GeP_2S_{12}$ Solid Electrolyte. *J. Power Sources* **2013**, *229*, 117−122.
(10) Wenzel, S.; Randau, S.; Leichtweiß, T.; Weber, D. A.; Sann, S.; Zeier, W. G.; Janek, J. Direct Observation of the Interfacial Instability of the Fast Ionic Conductor $Li_{10}GeP_2S_{12}$ at the Lithium Metal Anode. *Chem. Mater.* **2016**, *28*, 2400−2407.
(11) Hayashi, A.; Minami, K.; Ujiie, S.; Tatsumisago, M. Preparation and Ionic Conductivity of $Li_7P_3S_{11-z}$ Glass-Ceramic Electrolytes. *J. Non-Cryst. Solids* **2010**, *356*, 2670−2673.

DOI: 10.1021/acsenergylett.7b00319
ACS Energy Lett. 2017, 2, 1454−1459

(12) Wenzel, S.; Weber, D. A.; Leichtweiss, T.; Busche, M. R.; Sann, J.; Janek, J. Interphase Formation and Degradation of Charge Transfer Kinetics Between a Lithium Metal Anode and Highly Crystalline $Li_7P_3S_{11}$ Solid Electrolyte. *Solid State Ionics* **2016**, *286*, 24−33.
(13) Deiseroth, H.-J.; Kong, S.-T.; Eckert, H.; Vannahme, J.; Reiner, C.; Zaiβ, Y.; Schlosser, M. Li_6PS_5X: A Class of Crystalline Li-Rich Solids with an Unusually High Li^+ Mobility. *Angew. Chem., Int. Ed.* **2008**, *47*, 755−758.
(14) Rao, R. P.; Adams, S. Studies of Lithium Argyrodite Solid Electrolytes for All-Solid-State Batteries. *Phys. Status Solidi A* **2011**, *208*, 1804−1807.
(15) de Klerk, N. J. J.; Roslon, I.; Wagemaker, M. Diffusion Mechanism of Li Argyrodite Solid Electrolytes for Li-Ion Batteries and Prediction of Optimized Halogen Doping: The Effect of Li Vacancies, Halogens, and Halogen Disorder. *Chem. Mater.* **2016**, *28*, 7955−7963.
(16) Boulineau, S.; Tarascon, J.-M.; Leriche, J.-B.; Viallet, V. Electrochemical Properties of All-Solid-State Lithium Secondary Batteries Using Li-Argyrodite Li_6PS_5Cl as Solid Electrolyte. *Solid State Ionics* **2013**, *242*, 45−48.
(17) Mogensen, M. B.; Hennesø, E. Properties and Structure of the LiCl-films on Lithium Anodes in Liquid Cathodes. *Acta Chim. Slov.* **2016**, *63*, 519−534.
(18) Nazri, G. Preparation, Structure and Ionic Conductivity of Lithium Phosphide. *Solid State Ionics* **1989**, *34*, 97−102.
(19) Wu, B.; Wang, S.; Evans, W. J., IV; Deng, D. Z.; Yang, J.; Xiao, J. Interfacial Behaviours Between Lithium Ion Conductors and Electrode Materials in Various Battery Systems. *J. Mater. Chem. A* **2016**, *4*, 15266−15280.
(20) Ginnings, D. C.; Phipps, T. E. Temperature-Conductance Curves of Solid Salts. 111. Halides of Lithium. *J. Am. Chem. Soc.* **1930**, *52*, 1340−1345.
(21) Xue, Z.; He, D.; Xie, X. Poly(Ethylene Oxide)-Based Electrolytes for Lithium-Ion Batteries. *J. Mater. Chem. A* **2015**, *3*, 19218−19253.
(22) Irwin, M. T.; Hickey, R. J.; Xie, S.; So, S.; Bates, F. S.; Lodge, T. P. Structure−Conductivity Relationships in Ordered and Disordered Salt-Doped Diblock Copolymer/Homopolymer Blends. *Macromolecules* **2016**, *49*, 6928−6939.
(23) LaFemina, N. H.; Chen, Q.; Colby, R. H.; Mueller, K. T. The Diffusion and Conduction of Lithium in Poly(Ethylene Oxide)-Based Sulfonate Ionomers. *J. Chem. Phys.* **2016**, *145*, 114903.
(24) Safa, M.; Chamaani, A.; Chawla, N.; El-Zahab, B. Polymeric Ionic Liquid Gel Electrolyte for Room Temperature Lithium Battery Applications. *Electrochim. Acta* **2016**, *213*, 587−593.
(25) Simonetti, E.; Carewska, M.; Maresca, G.; De Francesco, M.; Appetecchi, G. B. Highly Conductive, Ionic Liquid-Based Polymer Electrolytes. *J. Electrochem. Soc.* **2017**, *164*, A6213−A6219.
(26) Kim, H. W.; Manikandan, P.; Lim, Y. J.; Kim, J. H.; Nam, S.; Kim, Y. Hybrid Solid Electrolyte with the Combination of $Li_7La_3Zr_2O_{12}$ Ceramic and Ionic Liquid for High Voltage Pseudo-Solid-State Li-ion Batteries. *J. Mater. Chem. A* **2016**, *4*, 17025−17032.

DOI: 10.1021/acsenergylett.7b00319
ACS Energy Lett. 2017, 2, 1454−1459